**Article:**
Guilbaud, R, Poulton, SW orcid.org/0000-0001-7621-189X, Butterfield, NJ et al. (2 more authors) (2015) A global transition to ferruginous conditions in the early Neoproterozoic oceans. Nature Geoscience, 8 (6). pp. 466-470. ISSN 1752-0908

https://doi.org/10.1038/ngeo2434

# A global transition to ferruginous conditions in the early Neoproterozoic oceans

Romain Guilbaud[1,2,*], Simon W. Poulton[1], Nicholas J. Butterfield[2], Maoyan Zhu[3], Graham A. Shields-Zhou[3,4]

[1]School of Earth and Environment, University of Leeds, Leeds LS2 9JT, UK

[2]Department of Earth Sciences, University of Cambridge, Cambridge CB2 3EQ, UK

[3]State Key Laboratory of Palaeobiology and Stratigraphy, Nanjing Institute of Geology and Paleontology, Nanjing 210008, China

[4]Department of Earth Sciences, University College London, London WC1E 6BT, UK

[*]corresponding author: r.j.guilbaud@leeds.ac.uk

**The Proterozoic Eon (2.5 to 0.542 billion years ago, Ga) is considered the cradle of eukaryotic life[1], but the impact of fluctuations in ocean chemistry on early eukaryote evolution is unclear[2–4]. After ~1.8 Ga, the global ocean is thought to have been dominated by oxygenated surface waters, overlying sulphidic mid-depth waters along productive ocean margins, and anoxic ferruginous (Fe-containing) deeper waters[5–7]. The spatial extent of sulphidic waters likely varied[5,6] but this redox structure is thought to have persisted until the first Neoproterozoic glaciation ~717 million years ago (Ma)[8–11]. Here, we utilise Fe-S systematics to assess ocean redox conditions across a suite of early Neoproterozoic successions (~1.0 to 0.717 Ga). Our data show a global transition from sulphidic to ferruginous mid-depth waters in the earliest Neoproterozoic, coincident with the amalgamation of the supercontinent Rodinia at low latitudes. We suggest that ferruginous conditions were initiated by an increase in the oceanic influx of highly reactive Fe relative to sulphate, driven by a change in weathering regime and the precipitation of extensive continental evaporites on Rodinia. After a prolonged period of relative evolutionary stasis, this 'detoxification' of ocean margin settings substantially expanded opportunities for eukaryotic diversification.**

Our understanding of the chemical evolution of the Precambrian ocean has altered dramatically over the last decade. It is now apparent that deep water ferruginous conditions were dominant throughout most of the Precambrian[5–8], at least until significant deep water oxygenation at ~0.58 Ga[8,12], although surface waters were partially oxygenated by ~2.7 Ga[13]. Progressive oxygenation of the atmosphere through the late Archaean and early Proterozoic resulted in higher input fluxes of

sulphate to the ocean due to oxidative weathering of continental sulphides[14]. This, in turn, favoured higher rates of bacterial sulphate reduction (BSR), leading to a significant increase in the extent of euxinic (anoxic and sulphidic) waters by ~1.8 Ga[5,14,15]. Euxinic conditions were particularly prevalent at mid-depths along productive continental margins and in intracratonic basins, but the deeper ocean remained ferruginous[5–7].

Although the spatial extent of euxinia may have varied[5,9,10], it is currently thought that this redox structure was dominant at least until the Sturtian Glaciation ~717 Ma[8,10]. Studies on later Neoproterozoic marine rocks have shown little evidence for euxinia from ~717 to 580 Ma, and instead, deeper waters were largely ferruginous[8,16]. Long-term ocean redox reconstructions are, however, hampered by a lack of data across key intervals[16], and this is particularly the case for the terminal Mesoproterozoic through the early Neoproterozoic (~1.1 to 0.74 Ga). This same interval witnessed a substantial increase in the diversity of fossil eukaryotes[1], but the connection to contemporaneous ocean chemistry remains unresolved. To evaluate ocean redox conditions in the early Neoproterozoic we have investigated marine successions from the north China craton (Huainan basin), Australia (Amadeus and Officer basins), Arctic Canada (Amundsen basin) and Spitsbergen (Svalbard basin, see Supplementary Information for full sample details and data). These new data are compiled with existing data to examine the redox evolution of the ocean from the late Palaeoproterozoic to the mid-Neoproterozoic.

Ocean redox chemistry was determined via iron speciation[17], whereby the biogeochemically highly reactive Fe pool ($Fe_{HR}$) is quantified relative to total Fe

71 ($Fe_T$). Anoxic water column settings promote $Fe_{HR}$ enrichments in the underlying
72 sediment, such that modern and ancient sediments deposited under anoxic conditions
73 typically display $Fe_{HR}/Fe_T$ >0.38 [6]. Sediments deposited under oxic water column
74 conditions lack $Fe_{HR}$ enrichments and are recognised by $Fe_{HR}/Fe_T$ ratios below 0.22
75 [6]. Ratios between 0.22-0.38 are considered equivocal[6], and may represent either
76 oxic or anoxic depositional conditions. In the latter case this may be due to the
77 masking of water column $Fe_{HR}$ enrichments by high sedimentation rates, or to
78 transformation of unsulfidized $Fe_{HR}$ to sheet silicate minerals during burial
79 diagenesis[5,18]. For unweathered, anoxic samples, ferruginous conditions are
80 distinguished from euxinic settings by quantifying the extent of sulphidation of the
81 highly reactive pool ($Fe_{py}/Fe_{HR}$). $Fe_{py}/Fe_{HR}$ >0.7-0.8 is characteristic of euxinic
82 deposition, whereas $Fe_{py}/Fe_{HR}$ <0.7 indicates deposition under ferruginous
83 conditions[6].
84
85 Our earliest Neoproterozoic samples represent an extensive, 700-800 m thick
86 succession of shales, siltstones, mudstones and carbonates from the ~1.0 Ga
87 Liulaobei, Jiuliqiao and Sidingshan Formations (Huainan and Feishui Groups,
88 Huainan region, north China craton). These sedimentary successions begin with
89 relatively deep-water continental slope deposits[19], but shallow upwards to intertidal
90 stromatolitic dolomites, and are thus ideal for identifying mid-depth redox conditions.
91 $Fe_{HR}/Fe_T$ ratios are dominantly above 0.38 (Fig. 1), indicating deposition under anoxic
92 water column conditions. The occasional occurrence of low $Fe_{HR}/Fe_T$ ratios likely
93 represents short-lived episodes of oxic deposition, perhaps reflecting storm events, or
94 fluctuations in the position of the chemocline. The entire set of anoxic samples has

95 $Fe_{py}/Fe_{HR}$ <0.7, demonstrating that the anoxic basin was characterised by ferruginous,
96 rather than euxinic, conditions.
97
98 Palaeogeographic reconstructions place the Huainan region at the northern tropical
99 periphery of Rodinia[20]. To obtain a global perspective we augmented these data with
100 new analyses of ~0.89-0.85 Ga shallow marine shales from the intracratonic
101 Amundsen basin (Arctic Canada) situated in the central eastern part of Rodinia,
102 ~0.84-0.77 Ga marine shales and carbonates from the intracratonic Amadeus and
103 Officer basins (Australia), situated in the northern part of Rodinia, and ~0.80 Ga
104 shallow marine shales from Svalbard (Spitsbergen), situated on the eastern periphery
105 of Rodinia (Supplementary Information). Most of these shallow marine samples are
106 consistent with deposition under oxic water column conditions, but those horizons
107 deposited under anoxic conditions are largely characterised by $Fe_{py}/Fe_{HR}$ <0.7 (Fig.
108 2), demonstrating that below the oxycline, waters were predominantly ferruginous.
109
110 We build upon these findings with a compilation of Fe speciation data, from the onset
111 of widespread mid-depth euxinia at ~1.8 Ga, through to the Sturtian Glaciation at
112 ~0.717 Ga (Table 1; Table S3). Whereas 12 out of 16 Palaeo-Mesoproterozoic
113 sections capturing anoxic, mid-depth settings show extensive evidence for euxinia
114 (173 out of 334 samples), only 16 samples spread across 3 of the 12 early
115 Neoproterozoic sections have $Fe_{py}/Fe_{HR}$ >0.8. Furthermore, these sixteen samples are
116 sporadically dispersed both temporally and spatially, suggesting either very short-
117 lived periods of water column euxinia[8,9,11] or extensive early diagenetic pyritization of
118 $Fe_{HR}$[10]. Regardless of the precise interpretation of these isolated samples, and in
119 contrast to earlier reports[8,9], we find no evidence for expanded euxinia in the early

120 Neoproterozoic ocean (Fig. 3). Instead, our dataset highlights a striking global change
121 from euxinic to ferruginous mid-depth waters around the Meso-Neoproterozoic
122 boundary.
123
124 This analysis suggests that ferruginous conditions, which were a prevalent feature of
125 deep waters during the later Neoproterozoic[8], dominated the entire ocean (beneath the
126 oxycline) throughout the early Neoproterozoic. The availability of organic carbon to
127 fuel BSR, after consumption by dissimilatory iron reduction, has been proposed as a
128 limiting factor in the development of euxinia in the Neoproterozoic ocean[10]. Low
129 organic carbon (TOC) contents throughout the Huainan basin section (<0.33 wt%,
130 Fig. 1) would be consistent with this view. However, ferruginous conditions were
131 prevalent in all of our studied basins, despite TOC contents (up to 0.84 wt%)
132 sufficient to support BSR. In addition, the rare samples with $Fe_{HR}/Fe_T$ >0.8 also have
133 very low TOC contents (<0.3 wt%). This suggests that the provision of organic
134 carbon was not the main factor controlling the chemical nature of water column
135 anoxia, and other mechanisms are required to explain the absence of mid-depth
136 euxinia during the early Neoproterozoic.
137
138 The oceanic budgets of $Fe_{HR}$ and sulphate, and relative changes in their influxes, have
139 also been proposed as a first order control on the chemical nature of water column
140 anoxia[6,8]. One mechanism to develop ferruginous conditions would be through low
141 atmospheric $pO_2$, thereby decreasing the sulphate influx from the oxidative
142 weathering of continental sulphides - but there is no evidence for a drop in $pO_2$ at this
143 time. However, a change in weathering regime may still have played a significant
144 role, as a consequence of the peneplanation of Rodinia which culminated shortly after

its amalgamation[21]. As supported by Sr isotope data[22], this resulted in diminished weathering fluxes at ~1 Ga. Hence, oceanic influxes of $Fe_{HR}$ and sulphate would have been considerably reduced at this time, making the response of ocean redox chemistry particularly sensitive to any proportional changes in their influx. Indeed, the change in weathering dynamics and sediment reworking induced by the peneplanation of Rodinia would have promoted a relative enhancement of chemical weathering over physical weathering. In addition to releasing both Fe and sulphate during pyrite oxidation, this results in a proportionately increased flux of $Fe_{HR}$ relative to sulphate via Fe release from parent silicate minerals[18].

A dramatic 15-fold increase in the volume of evaporites (many of which are sulphate-bearing) on intracontinental basins (Fig. 3) following the amalgamation of Rodinia at low latitudes[23], would also have impacted the sulphur cycle. Sulphur isotope fractionations between seawater sulphate and pyrite ($\Delta^{34}S_{CAS\text{-}pyrite}$) of <20‰ in the Bitter Springs and Finke Beds formations (Amadeus basin), and analysis of halite fluid inclusions (Officer basin), suggest that sulphate concentrations in intracratonic basins were in the low millimolar range at ~0.81-0.77 Ga [24,25]. This is supported by our sulphur isotope data for the open marine Huainan basin (Fig. 1). Relatively heavy $\delta^{34}S_{pyrite}$ values coupled with very low pyrite contents ($Fe_{Py}$ = 0.04 wt% on average) indicate near quantitative sulphate reduction from a small seawater sulphate reservoir. In the lower part of the section, $\delta^{34}S_{pyrite}$ is heavier than $\delta^{34}S_{CAS}$ (Fig. 1). Whilst this could reflect a series of Rayleigh-like fractionations during minor sulphide re-oxidation[26], or perhaps some influence from modern atmospheric pollution on outcrop samples[27], the data are entirely consistent with very low sulphate concentrations. Towards the top of the Huainan succession, $\delta^{34}S_{CAS}$ is enriched

relative to $\delta^{34}S_{pyrite}$ in the shallower water carbonates. Utilizing a simple sulphur isotope box model (Supplementary Information), these data support very low seawater sulphate concentrations in the early Neoproterozoic, and perhaps even a decrease in concentrations if estimates[28] at ~1.1 Ga [29] are correct (Fig. 3). Since this time period appears to be characterised by low pyrite burial (Fig. 1), these observations suggest that the oceanic influx of sulphate was particularly low during the early Neoproterozoic.

In light of these data, the initiation of the late Mesoproterozoic transition from euxinic to ferruginous mid-depth waters was most likely a consequence of an increased $Fe_{HR}$[6] influx relative to sulphate, rather than a global change in organic C availability. Controls on the persistence of ferruginous conditions up until the Sturtian glaciation (and beyond)[8] as Rodinia broke up are less clear. However, increased chemical weathering fluxes during continental breakup would also have favoured an enhanced influx of $Fe_{HR}$ relative to sulphate, which would have helped maintain ferruginous water column conditions throughout the early Neoproterozoic.

Our results refine current understanding of ocean redox evolution during the Proterozoic, for the first time highlighting a retraction of $H_2S$-rich anoxia in mid-depth waters prior to the first Cryogenian glaciation. In addition to providing a more complete understanding of the environmental context that presaged the first Neoproterozoic 'snowball' Earth glaciation, this transition likely had consequences for biological evolution. There is a widespread capacity for anaerobic (and sulphide) metabolism amongst major eukaryotic groups[4,30]. However, periodic incursions of toxic levels of sulphide into oxygenated, eukaryote-harbouring shallow waters, due to

temporal variability in the position of the oxycline, likely presented a major constraint on the evolutionary expansion of aerobic eukaryotes. This may explain why, prior to ~1.0 Ga, eukaryotic biology is marked by its modest diversity and relative evolutionary stasis (Fig. 3). The broad transition from Mesoproterozoic *Tappania*/*Grypania*-dominated assemblages[31] to Neoproterozoic *Trachyhystrichosphaera*/*Tawuia*-dominated ones[19] could well be related to the decrease in euxinic mid-depth waters initiated by the assembly of Rodinia. The global expansion and persistence of ferruginous mid-depth waters also witnessed an early Neoproterozoic increase in acritarch diversity[1] (Fig. 3). Thus, whereas incursions of sulphide into oxygenated shallow waters may have placed significant constraints on eukaryote evolution in the earlier Proterozoic[5], terminal Mesoproterozoic to early Neoproterozoic shallow waters were essentially 'detoxified' for a period of several hundred million years in the prelude to the Sturtian 'snowball' glaciation. We suggest that this ocean 'detoxification' opened up significant new ecospace for aerobic eukaryotes, presaging the revolutionary innovations of the middle and late Neoproterozoic.

## References


1. Knoll, A. H., Javaux, E. J., Hewitt, D. & Cohen, P. Eukaryotic organisms in Proterozoic oceans. *Philosophical Transactions of the Royal Society B: Biological Sciences* **361,** 1023–1038 (2006).
2. Anbar, A. D. & Knoll, A. Proterozoic ocean chemistry and evolution: a bioinorganic bridge? *Science* **297,** 1137–1142 (2002).

3. Lenton, T. M., Boyle, R. A., Poulton, S. W., Shields-Zhou, G. A. & Butterfield, N. J. Co-evolution of eukaryotes and ocean oxygenation in the Neoproterozoic era. *Nature Geosci* **7,** 257–265 (2014).
4. Mentel, M. & Martin, W. Energy metabolism among eukaryotic anaerobes in light of Proterozoic ocean chemistry. *Philosophical Transactions of the Royal Society B: Biological Sciences* **363,** 2717–2729 (2008).
5. Poulton, S. W., Fralick, P. W. & Canfield, D. E. Spatial variability in oceanic redox structure 1.8 billion years ago. *Nature Geosci* **3,** 486–490 (2010).
6. Poulton, S. W. & Canfield, D. E. Ferruginous Conditions: A Dominant Feature of the Ocean through Earth's History. *Elements* **7,** 107–112 (2011).
7. Planavsky, N. J. *et al.* Widespread iron-rich conditions in the mid-Proterozoic ocean. *Nature* **477,** 448–451 (2011).
8. Canfield, D. E. *et al.* Ferruginous Conditions Dominated Later Neoproterozoic Deep-Water Chemistry. *Science* **321,** 949–952 (2008).
9. Dahl, T. W. *et al.* Molybdenum evidence for expansive sulfidic water masses in~ 750Ma oceans. *Earth and Planetary Science Letters* **311,** 264–274 (2011).
10. Johnston, D. T. *et al.* An emerging picture of Neoproterozoic ocean chemistry: Insights from the Chuar Group, Grand Canyon, USA. *Earth and Planetary Science Letters* **290,** 64–73 (2010).
11. Thomson, D., Rainbird, R. H., Planavsky, N., Lyons, T. W. & Bekker, A. Chemostratigraphy of the Shaler Supergroup, Victoria Island, NW Canada: A record of ocean composition prior to the Cryogenian glaciations. *Precambrian Research* doi:10.1016/j.precamres.2015.02.007
12. Canfield, D. E., Poulton, S. W. & Narbonne, G. M. Late-Neoproterozoic Deep-Ocean Oxygenation and the Rise of Animal Life. *Science* **315,** 92–95 (2007).

13. Kendall, B. *et al.* Pervasive oxygenation along late Archaean ocean margins. *Nature Geosci* **3,** 647–652 (2010).

14. Canfield, D. E. A new model for Proterozoic ocean chemistry. *Nature* **396,** 450–453 (1998).

15. Poulton, S. W., Fralick, P. W. & Canfield, D. E. The transition to a sulphidic ocean 1.84 billion years ago. *Nature* **431,** 173–177 (2004).

16. Raiswell, R. & Canfield, D. E. The iron biogeochemical cycle past and present. *Geochemical Perspectives* **1,** 1–2 (2012).

17. Poulton, S. W. & Canfield, D. E. Development of a sequential extraction procedure for iron: implications for iron partitioning in continentally derived particulates. *Chemical Geology* **214,** 209–221 (2005).

18. Poulton, S. W. & Raiswell, R. The low-temperature geochemical cycle of iron: From continental fluxes to marine sediment deposition. *Am J Sci* **302,** 774–805 (2002).

19. Tang, Q. *et al.* Organic-walled microfossils from the early Neoproterozoic Liulaobei Formation in the Huainan region of North China and their biostratigraphic significance. *Precambrian Research* **236,** 157–181 (2013).

20. Li, Z.-X., Evans, D. A. D. & Halverson, G. P. Neoproterozoic glaciations in a revised global palaeogeography from the breakup of Rodinia to the assembly of Gondwanaland. *Sedimentary Geology* **294,** 219–232 (2013).

21. Spencer, C. J. *et al.* Proterozoic onset of crustal reworking and collisional tectonics: Reappraisal of the zircon oxygen isotope record. *Geology* **42,** 451–454 (2014).

22. Shields, G. A normalised seawater strontium isotope curve: possible implications for Neoproterozoic-Cambrian weathering rates and the further oxygenation of the Earth. *eEarth* **2,** 35–42 (2007).

23. Evans, D. A. D. Proterozoic low orbital obliquity and axial-dipolar geomagnetic field from evaporite palaeolatitudes. *Nature* **444,** 51–55 (2006).

24. Gorjan, P., Veevers, J. & Walter, M. Neoproterozoic sulfur-isotope variation in Australia and global implications. *Precambrian Research* **100,** 151–179 (2000).

25. Spear, N. *et al.* Analyses of fluid inclusions in Neoproterozoic marine halite provide oldest measurement of seawater chemistry. *Geology* **42,** 103–106 (2014).

26. Ries, J. B., Fike, D. A., Pratt, L. M., Lyons, T. W. & Grotzinger, J. P. Superheavy pyrite (δ34Spyr > δ34SCAS) in the terminal Proterozoic Nama Group, southern Namibia: A consequence of low seawater sulfate at the dawn of animal life. *Geology* **37,** 743–746 (2009).

27. Peng, Y. *et al.* Widespread contamination of carbonate-associated sulfate by present-day secondary atmospheric sulfate: Evidence from triple oxygen isotopes. *Geology* (2014). doi:10.1130/G35852.1

28. Kah, L. C., Lyons, T. W. & Frank, T. D. Low marine sulphate and protracted oxygenation of the Proterozoic biosphere. *Nature* **431,** 834–838 (2004).

29. Geboy, N. J. *et al.* Re–Os age constraints and new observations of Proterozoic glacial deposits in the Vazante Group, Brazil. *Precambrian Research* **238,** 199–213 (2013).

30. Embley, T. M. Multiple secondary origins of the anaerobic lifestyle in eukaryotes. *Philosophical Transactions of the Royal Society B: Biological Sciences* **361,** 1055–1067 (2006).

31. Adam, Z. R., Mogk, D. W., Skidmore, M. & Butterfield, N. J. Microfossils from the Greyson Formation, Lower Belt Supergroup: support for early Mesoproterozoic biozonation. *Geological Society of America Abstracts with Programs* **46,** 71 (2014).

## Methods

All data are reported in Table S1. The iron speciation method was performed following well-established Fe sequential extraction schemes[17] which target operationally defined Fe pools, including carbonate associated-Fe ($Fe_{Carb}$), ferric oxides-Fe ($Fe_{Ox}$), magnetite-Fe ($Fe_{Mag}$), pyrite-Fe ($Fe_{Py}$), poorly reactive sheet silicates-Fe ($Fe_{PRS}$) and total Fe ($Fe_T$). Total Fe ($Fe_T$) was extracted by a $HNO_3$-HF-$HClO_4$-$H_3BO_3$-HCl sediment digestion. Most of our samples were marine shales, but for the occasional carbonate-rich samples, Fe sequential extractions were performed on samples with $Fe_T$ contents >0.5 wt%, as suggested by a recent calibration for carbonate samples[32]. Highly reactive Fe ($Fe_{HR}$) is calculated as $Fe_{HR} = Fe_{Carb} + Fe_{Ox} + Fe_{Mag} + Fe_{Py}$. $Fe_{Carb}$, $Fe_{Ox}$, and $Fe_{Mag}$ were extracted sequentially by a sodium acetate leach (48 h at 50°C), followed by a sodium dithionite leach (2 h at ambient temperature) and an ammonium oxalate leach (6 h at ambient temperature)[17]. [Fe] in each extract was measured by Atomic Absorption Spectroscopy and replicate analysis gave a RSD <4% for each step, leading to <8% for calculated $Fe_{HR}$, which is comparable to the precision obtained by other laboratories[17]. The final fraction of $Fe_{HR}$, ($Fe_{Py}$) was calculated from the wt% of sulphide extracted as $Ag_2S$ using hot $Cr(II)Cl_2$ distillation[33]. A boiling HCl distillation prior to the $Cr(II)Cl_2$ distillation ruled out the potential presence of acid volatile sulphides in our samples. Pyrite-S was determined on $Ag_2S$ precipitates from the $Cr(II)Cl_2$ distillation. Analysis of a certified

316 reference material (PACS-2, $Fe_T$ = 3.96 ± 0.10 wt%, *n* = 16; certified value = 4.09 ±
317 0.06 wt%) confirms that our method is accurate. Replicate analyses (*n* = 10) gave a
318 precision of ± 0.04 on the $Fe_{HR}/Fe_T$ ratio.
319
320 TOC was determined by the difference between total carbon (TC) before and after
321 inorganic carbon removal (two 25% (vol/vol) HCl washes for 24 hours). Samples
322 were analysed on a LECO® carbon analyser and replicate analyses gave a precision of
323 ± 0.09 wt% (2σ level).
324
325 CAS was extracted from 10-20 g of carbonate-rich samples following recently refined
326 techniques[34]. Samples were washed twice with 5% NaOCl for 24 h to remove
327 sulphide and organic S, followed by at least three washes in 10% NaCl for 24 h to
328 remove soluble sulphate. Additional NaCl washes were performed when $BaSO_4$
329 precipitated upon addition of excess $BaCl_2$ to the filtrate. CAS was extracted by
330 carbonate dissolution in 10% v/v HCl and precipitated as $BaSO_4$ by addition of excess
331 $BaCl_2$ at pH 2.5. S isotope analyses were performed on $Ag_2S$ and $BaSO_4$ precipitates
332 by Iso-Analytical Ltd., UK, and all data are reported with respect to the Vienna
333 Canyon Diablo Troilite standard (V-CDT). Replicate analysis led to a precision of ±
334 0.10‰ (1σ level) for $BaSO_4$ and ± 0.24‰ for $Ag_2S$ (*n* = 7).
335
336 Our Fe speciation results (n = 226) were combined with 789 literature data from
337 anoxic settings ranging from 1.878 to 0.742 Ga (Fig. 3; Table 1). Compiled data
338 (Table S3) come from the ~1.8 Ga Animikie basin[5,15], the 1.86 Ga Koolpin Formation
339 (Poulton, in prep.), the 1.7 Ga Lower Changcheng Group[7], the 1.64 Ga Mt. Isua
340 Superbasin[7], the 1.45 Ga Lower Belt Supergroup[7], the 1.4 Ga Roper basin[35], the 1.2

Ga Bylot Supergroup[7], the 1.1 Ga Vazante Group[29], the 1.1 Ga Taoudeni basin[36], the ~1.0 Ga Feishui Group (this study), the ~1.0 Ga Huainan Group (this study), the ~0.89-0.80 Ga Reynolds Point and Wynniatt Formations (Amundsen basin, this study and ref [11]), the ~0.84-0.77 Ga Amadeus and Officer basins (Australian Centralian basin, this study), the ~0.81 Ga Fifteenmile Group[37], the 0.742 Ga Chuar Group[10] and the ~0.74 Ga Svanbergfjellet Formation (Spitsbergen, this study).

$Fe_{Py}/Fe_{HR}$ was used as a reflection of the distribution of euxinia through time. Fig. 3 distinguishes between "shallow/mid-depth" and "deep" environments as described in the original source. "Shallow/mid-depth environments" include i) continental margins and proximal deposits[5,7,15,29,35,37], and ii) epicontinental seas and intracratonic basins[10,36,38]. "Deep environments" include settings showing evidence for deposition below the storm wave base or distal sediments[7,13,35,37]. Table 1 shows the distribution of $Fe_{Py}/Fe_{HR}$ within the dataset. Note that before 1 Ga, $Fe_{Py}/Fe_{HR}$ is on average 0.12 for deep waters and 0.68 for shallow waters (median of 0.75), which includes samples that were deposited before the transition to widespread euxinia at ~1.8 Ga, as recorded in the Animikie basin[5,15], whereas after 1 Ga, $Fe_{Py}/Fe_{HR}$ is on average 0.06 for deep waters and 0.17 for shallow waters.

**Methods references**

32. Clarkson, M., Poulton, S., Guilbaud, R. & Wood, R. Assessing the utility of Fe/Al and Fe-speciation to record water column redox conditions in carbonate-rich sediments. *Chemical Geology* (2014).

33. Canfield, D. E., Raiswell, R., Westrich, J. T., Reaves, C. M. & Berner, R. A. The use of chromium reduction in the analysis of reduced inorganic sulfur in sediments and shales. *Chemical Geology* **54,** 149–155 (1986).

34. Goldberg, T., Shields, G. A. & Newton, R. J. Analytical constraints on the measurement of the sulfur isotopic composition and concentration of trace sulfate in phosphorites: implications for sulfur isotope studies of carbonate and phosphate rocks. *Geostandards and Geoanalytical Research* **35,** 161–174 (2011).

35. Shen, Y., Knoll, A. H. & Walter, M. R. Evidence for low sulphate and anoxia in a mid-Proterozoic marine basin. *Nature* **423,** 632–635 (2003).

36. Gilleaudeau, G. J. & Kah, L. C. Oceanic molybdenum drawdown by epeiric sea expansion in the Mesoproterozoic. *Chemical Geology* **356,** 21–37 (2013).

37. Sperling, E. A., Halverson, G. P., Knoll, A. H., Macdonald, F. A. & Johnston, D. T. A basin redox transect at the dawn of animal life. *Earth and Planetary Science Letters* (2013).

38. Shen, Y., Canfield, D. E. & Knoll, A. H. Middle Proterozoic ocean chemistry: evidence from the McArthur Basin, northern Australia. *American Journal of Science* **302,** 81–109 (2002).

Correspondence and requests for material should be addressed to R. Guilbaud.

**Acknowledgements**

We are thankful to Phil Green, Jane Davis and Eva Avbelj for technical support. We thank Simon Bottrell and Robert Newton, and three anonymous reviewers for constructive discussions. This work was supported by NERC through its research program “Long-term Co-evolution of Life and the Planet” (Project NE/I005978/1),

and the 973 program of the Ministry of Science and Technology of China (2013CB835000).

**Author contributions**

RG, SWP, GSZ and MZ collected samples. RG analysed samples and interpreted data. RG and SWP wrote the manuscript, with significant contributions from all co-authors.

**Table captions**

**Table 1:** Statistical analysis of the distribution of $Fe_{Py}/Fe_{HR}$ within a compilation of shallow to mid-depth, anoxic settings, ranging from 2 Ga to the Sturtian. A full description of the compilation is available in the method section. For samples >1.0 Ga, $Fe_{Py}/Fe_{HR}$ is on average 0.68 ± 0.27 (median = 0.75), whereas for samples <1.0 Ga, it is 0.17 ± 0.28 (median = 0.01). T-test analysis led to a p-value <<0.01, suggesting that the averages of each groups are significantly different. Twenty sets of randomly generated resampled data (with data replacement) average at 0.68 ± 0.09 for samples >1.0 Ga, and at 0.18 ± 0.11 for samples <1.0 Ga.

**Figure captions**

**Figure 1**: Stratigraphy and geochemical analyses for the ~1.0 Ga Huainan succession. S isotope compositions of pyrite (black circles) and coeval CAS (grey circles) are also given. The red bands correspond to averages in $\delta^{34}S_{pyrite}$ used in the S isotope model (see main text and SI for a full description).

**Figure 2**: Fe speciation data for the ~1.0 Ga Huainan basin, the ~0.89-0.79 Ga Amundsen basin, the ~0.84-0.77 Ga Amadeus and Officer basins, and the 0.74 Ga Svalbard basin. Most samples from the Amundsen, Amadeus and Officer basins are from shallow settings, and the data plot mostly within the oxic domain. Anoxic samples from all basins plot dominantly within the anoxic, ferruginous domain.

**Figure 3**: Data compilation from 2 Ga to the Sturtian glaciation. i) Ocean redox structure through time; ii) $Fe_{Py}/Fe_{HR}$ data for available anoxic samples. Mid-depth environments are represented by squares, deeper environments by small circles. Red denotes ferruginous ($Fe_{Py}/Fe_{HR}$ <0.8) and grey denotes euxinic conditions ($Fe_{Py}/Fe_{HR}$ >0.8. Darker colours illustrate the interquartile range. Open squares denote the average values and standard deviations for mid-depth samples before and after 1 Ga. iii) Modelled estimates of seawater sulphate concentration. Open circles are from ref. [28], with the age of the ~1.1 Ga data based on recent reappraisals[29]. The red circle represents our study; iv) Evaporite record (from ref. [23]); v) Acritarch taxa per assemblage record (after ref. [1]) and the transition in fossil assemblages.

Table 1: Literature compilation of FePy/FeHR as an indicator for euxinic settings within anoxic basins from 1.88 Ga to 0.74 Ga.

| Age (Ga) | Formation | n | mean | min | max | quartile 1 | median | quartile 3 |
|---|---|---|---|---|---|---|---|---|
| 1.878 | Animikie Basin, deep and distal deposits | 127 | 0.03 | 0.00 | 0.68 | 0.00 | 0.00 | 0.02 |
| 1.86 | Koolpin Formation, Pine Creek | 23 | 0.89 | 0.74 | 0.99 | 0.83 | 0.87 | 0.96 |
| 1.835 | Animikie Basin, deep and distal deposits | 82 | 0.16 | 0.00 | 0.61 | 0.04 | 0.13 | 0.24 |
| 1.835 | Animikie Basin, shallow and proximal deposits | 152 | 0.55 | 0.08 | 0.95 | 0.37 | 0.51 | 0.75 |
| 1.7 | Lower Changcheng group (Jixian Region), deep deposits | 21 | 0.22 | 0.01 | 0.49 | 0.16 | 0.23 | 0.27 |
| 1.64 | Mt. Isua Superbasin, shallow deposits | 52 | 0.52 | 0.00 | 0.96 | 0.37 | 0.50 | 0.69 |
| 1.45 | Lower Belt Supergroup, deep deposits | 11 | 0.54 | 0.19 | 0.83 | 0.42 | 0.52 | 0.69 |
| 1.4 | Roper Basin, shallow deposits | 22 | 0.92 | 0.78 | 0.97 | 0.90 | 0.92 | 0.94 |
| 1.2 | Bylot Supergroup, shallow deposits | 4 | 0.53 | 0.45 | 0.59 | - | - | - |
| 1.1 | Vazante Group, shallow deposits | 78 | 0.92 | 0.10 | 1.00 | 0.92 | 0.97 | 0.98 |
| 1.1 | Taoudeni Basin, shallow deposits | 36 | 0.51 | 0.00 | 0.97 | 0.18 | 0.50 | 0.82 |
| ~1.0 | Feishui Group, shallow deposits | 63 | 0.04 | 0.00 | 0.31 | 0.00 | 0.00 | 0.03 |
| ~1.0 | Huainan Group, deeper deposits | 53 | 0.00 | 0.00 | 0.05 | 0.00 | 0.00 | 0.00 |
| 0.89 | Reynolds Point formation, shallow shales | 6 | 0.02 | 0.00 | 0.62 | 0.00 | 0.00 | 0.01 |
| 0.81-0.79 | Amadeus Basin, shallow deposits | 9 | 0.40 | 0.02 | 0.81 | 0.14 | 0.34 | 0.60 |
| 0.81 | Fifteenmile Group, deep deposits | 100 | 0.09 | 0.00 | 0.73 | 0.00 | 0.02 | 0.09 |
| 0.81 | Fifteenmile Group, shallow deposits | 8 | 0.00 | 0.00 | 0.00 | - | - | - |
| 0.8 | Wynniatt formation, shallow shales | 17 | 0.65 | 0.00 | 0.93 | 0.53 | 0.78 | 0.82 |
| 0.77 | Hussar and Kanpa formations, shallow sediments | 5 | 0.20 | 0.00 | 0.86 | 0.00 | 0.03 | 0.14 |
| 0.74 | Svanbergfjellet formation, shallow shales | 3 | 0.45 | 0.23 | 0.46 | - | - | - |
| 0.742 | Chuar Group, shallow and deep sediments | 60 | 0.15 | 0.00 | 0.90 | 0.00 | 0.00 | 0.18 |
| | | Sum 932 | | | | | | |

| Age (Ga) | Formation | n | mean | std | median |
|---|---|---|---|---|---|
| >1.1 | Proximal, shallow to mid-depth samples | 334 | 0.68 | 0.27 | 0.75 |
| | Randomly generated resampled data | 20 x 30 | 0.68 | 0.09 | |
| <1.1 | Proximal, shallow to mid-depth samples | 171 | 0.17 | 0.28 | 0.01 |
| | Randomly generated resampled data | 20 x 17 | 0.18 | 0.11 | |

**Figure 1.**

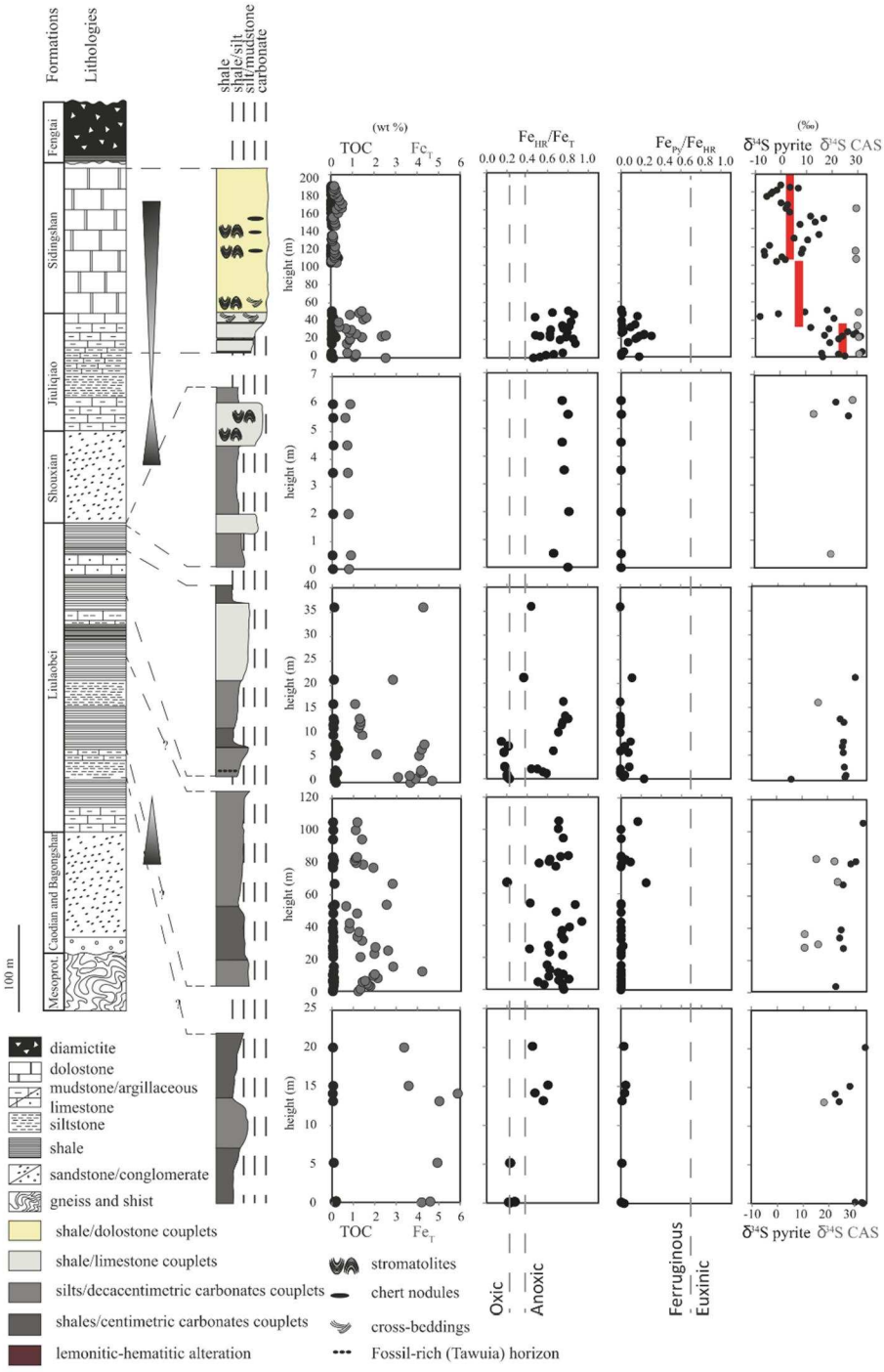
Formations
Lithologies
shale
shale/silt
siltstone
carbonate
Fengtai
Sidingshan
Jiuliqiao
Shouxian
Liulaobei
Caodian and Bagongshan
Mesoprot.
100 m
(wt %)
TOC
$Fe_T$
$Fe_{HR}/Fe_T$
$Fe_{py}/Fe_{HR}$
(‰)
$\delta^{34}S$ pyrite
$\delta^{34}S$ CAS
height (m)
diamictite
dolostone
mudstone/argillaceous
limestone
siltstone
shale
sandstone/conglomerate
gneiss and shist
shale/dolostone couplets
shale/limestone couplets
silts/decacentimetric carbonates couplets
shales/centimetric carbonates couplets
lemonitic-hematitic alteration
stromatolites
chert nodules
cross-beddings
Fossil-rich (Tawuia) horizon
Oxic
Anoxic
Ferruginous
Euxinic

**Figure 2.**

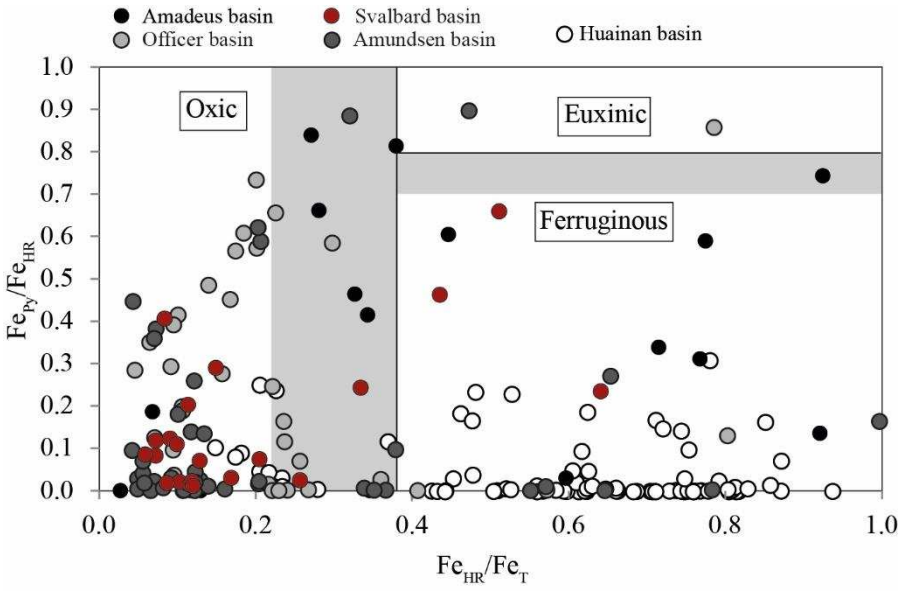
Amadeus basin
Officer basin
Svalbard basin
Amundsen basin
Huainan basin
Oxic
Euxinic
Ferruginous
$Fe_{Py}/Fe_{HR}$
$Fe_{HR}/Fe_T$
0.0
0.1
0.2
0.3
0.4
0.5
0.6
0.7
0.8
0.9
1.0
0.0
0.2
0.4
0.6
0.8
1.0

**Figure 3.**

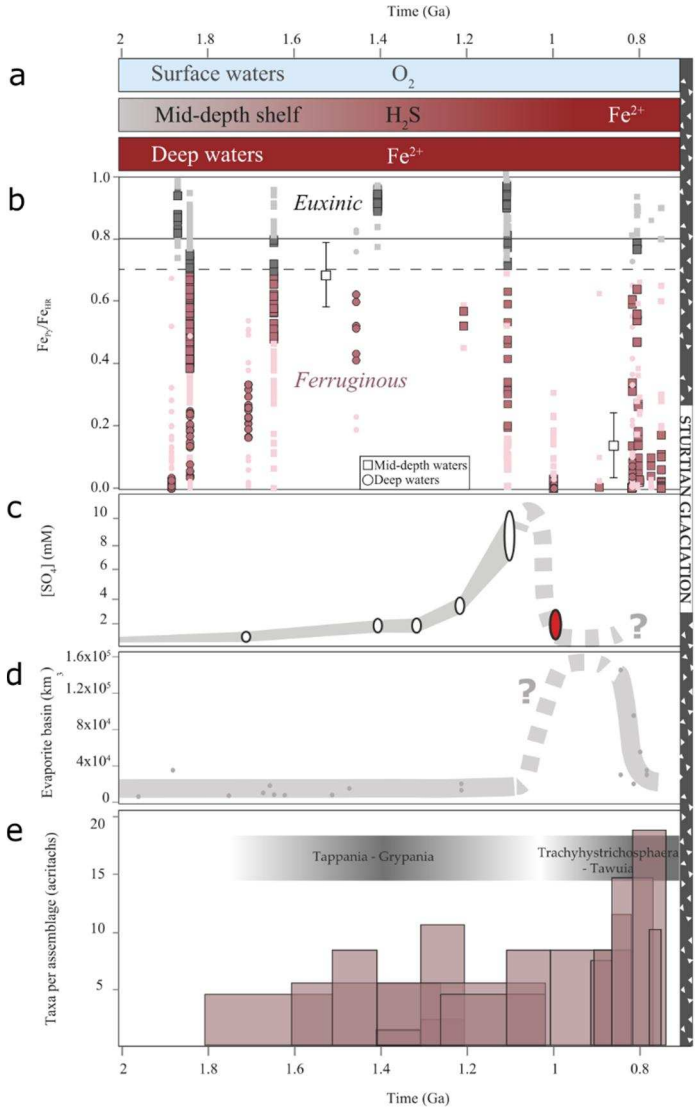
Time (Ga)
2
1.8
1.6
1.4
1.2
1
0.8
a
Surface waters
$O_2$
Mid-depth shelf
$H_2S$
$Fe^{2+}$
Deep waters
$Fe^{2+}$
b
Euxinic
Ferruginous
$Fe_{py}/Fe_{HR}$
Mid-depth waters
Deep waters
STURTIAN GLACIATION
c
$[SO_4]$ (mM)
?
d
Evaporite basin ($km^3$)
?
e
Taxa per assemblage (acritachs)
Tappania - Grypania
Trachyhystrichosphaera - Tawuia
Time (Ga)